Investigation of the $6s6p\,^3P_0 - 4f^{13}5d6s^2$ $(J=2)$ Clock Transition in ^{171}Yb Atoms

Hao Qiao,[1,*] Di Ai,[1,*] Chang-Yue Sun,[1] Cheng-Quan Peng,[1] Qi-Chao Qi,[1] Cheng-Cheng Zhao,[1] Li-Meng Luo,[1] Tao-Yun Jin,[1] Tao Zhang,[1] Min Zhou,[1] and Xin-Ye Xu[1,2,†]

[1]*State Key Laboratory of Precision Spectroscopy, East China Normal University, Shanghai 200062, People's Republic of China*

[2]*Shanghai Research Center for Quantum Sciences, Shanghai 201315, China*

(Received 11 May 2023; accepted 3 January 2024; published 20 February 2024)

High-precision atomic spectroscopy provides an invaluable and sensitive tool for exploring a wide range of physical questions. Here, we investigate the forbidden optical transition of the $6s6p^3P_0 - 4f^{13}5d6s^2$ $(J=2)$ in ^{171}Yb atoms at the wavelength of 1695 nm, which exhibits the highest sensitivity to the variation of the fine-structure constant α compared to the current neutral optical clock. We obtain high-resolution transition spectroscopy in a one-dimensional optical lattice, and the measurement of its absolute frequency achieves kHz-level accuracy. Meanwhile, several essential atomic constants are also determined, including the electric-dipole ($E1$) magic wavelengths, as well as the hyperpolarizabilities and tensor polarizabilities around the $E1$ magic wavelengths. Additionally, we derive the hyperfine constant for the $J=2$ state from the measured absolute frequencies $1123\,252.3 \pm 2.0$ kHz, providing a sixfold enhancement in the uncertainty reduction compared to the recent result. We anticipate that this work will prompt further investigation of the additional clock transition at 1695 nm in ^{171}Yb atoms. Together with the well-established $^1S_0$-$^3P_0$ transition, many fundamental and new physics research, such as the time variation of α, ultralight dark-matter searches, Lorentz violation, etc., will enable new bounds and measurements with unprecedented precision.

DOI: 10.1103/PhysRevX.14.011023

Subject Areas: Atomic and Molecular Physics, Optics, Quantum Physics

I. INTRODUCTION

Atoms with two valence electrons, such as the alkaline earth metals ytterbium (Yb), possess ultranarrow transitions from their ground state to metastable states [1–5]. Currently, several groups have recognized ytterbium as an excellent candidate for redefining the Systeme International (SI) second, and have achieved significant advancements in lattice-based optical clocks utilizing its ultranarrow $^1S_0$-$^3P_0$ transition [6–13], which exhibits insensitivity to most environmental effects. Over the past two decades, the development of the optical atomic clocks has made a factor of more than 10^3 improvement in precision, and they have now reached unrivaled inaccuracy and instability at the low 10^{-18} level [6,14–18]. Consequently, optical lattice clocks are extensively employed to perform more stringent tests of fundamental physical principles and to advance applications in fields such as quantum simulations [19–22], gravitational-wave detection [23–25], relativistic geodesy [18,26–28], searches for temporal drifts in the fundamental constants [16,29–31], dark-matter searches [32,33], tests of the Lorentz invariance [34,35], the redefinition of the second [36,37], etc.

In the neutral Yb atom, several metastable states exist, such as the $6s6p\,^3P_{0,2}$ and $4f^{13}5d6s^2$ $(J=2)$ states, which are anticipated to be applied to the development of new clock transitions [38,39]. The $6s6p^3P_{0,2}$ states have been thoroughly investigated experimentally, whereas the $4f^{13}5d6s^2$ $(J=2)$ state has not yet garnered comparable attention. The electronic configuration of the $J=2$ state featuring an open f shell and a single $5d$ electron bears similarity to the $\mathrm{Yb}^+ {}^2S_{1/2} - {}^2D_{3/2}(E2)$ and ${}^2S_{1/2} - {}^2F_{7/2}(E3)$ transitions [31]. Recently, several research groups have suggested that the $6s6p^3P_0 - 4f^{13}5d6s^2$ $(J=2)$ transition at 1695-nm wavelength in the Yb atom has the potential for achieving high stability and accuracy [38,39]. Therefore, combining the other well-established $6s^2\,{}^1S_0 - 6s6p\,{}^3P_0$ transition for clock-comparison experiments could reduce the systematic uncertainties, such as the blackbody radiation (BBR) effect [40,41]. Additionally, the transition exhibits significant sensitivity to temporal variations in the fine-structure constant α and local Lorentz

*These authors contributed equally to this work.

†Corresponding author: xyxu@phy.ecnu.edu.cn

invariance violation. Theoretical calculations and analyses reveal that the dimensionless α-variation enhancement factor of the transition for Yb is approximately -15 [38], which is much larger than any other currently operating optical atomic clocks [42]. For instance, comparison with the standard clock transition in Yb of approximately 0.36 indicates that the 1695-nm transition displays over 40 times greater sensitivity than the $^1S_0$-$^3P_0$ clock transition, given comparable fractional stability and accuracy. Hence, it is proposed that this clock transition could be used for studies of fundamental physics.

Currently, the $E3$ transition in Yb^+ represents the most well-established transition for testing α variations, boasting an enhancement factor of approximately 6. When compared to transitions in Yb^+ optical clocks, the enhanced sensitivity of the 1695-nm transition does not significantly surpass that of the $E3$ transition. Furthermore, it may present challenges in achieving the comparable levels of systematic uncertainty currently demonstrated by Yb^+ clocks [16]. However, the 1695-nm transition offers a distinct stability advantage over the Yb^+ optical clock owing to its ability to operate with a larger number of atoms, which proves pivotal in detecting transient or oscillating changes in α. Similarly, when comparing the 1695-nm transition with the 431-nm transition [39], given that the considerable sensitivity of the 1695-nm transition is attributable to the $J = 2$ excited state's susceptibility to α variations, both the $^1S_0$-$J = 2$ and $^3P_0$-$J = 2$ transitions in Yb exhibit nearly identical sensitivities to the absolute frequency shifts resulting from α changes, as posited in Refs. [38,39] to investigate temporal variations of α. The difference in enhancement factors between the two transitions pertains exclusively to their distinct transition frequencies. Nonetheless, the 1695-nm transition retains an advantage regarding absolute frequency stability, should the clock-laser coherence time constitute a limitation to stability.

Undoubtedly, the 1695-nm transition exhibits a considerable sensitivity to environmental influences like the Zeeman effect, attributable to its nonzero total electronic angular momentum $J = 2$. This sensitivity could potentially limit accuracy under conventional experimental conditions and might also diminish the transition's relative advantages in α-variation sensitivity when contrasted with established optical clocks. However, several methods are available that can experimentally address and mitigate challenges related to the 1695-nm transition; for instance, employing magnetic shielding can reduce the large Zeeman shift. Whether the loss in clock performance eliminates the sensitivity advantage entirely in α variations is an outstanding question that likely can be resolved only through experimental inquiry.

The 1695-nm transition in the ^{171}Yb atom is an electric-quadrupole ($E2$) transition. The lower ground state $6s6p\ ^3P_0$ is a metastable state with a lifetime of approximately 20 s, while the upper excited state $4f^{13}5d6s^2$ $(J = 2)$ has a lifetime of more than one minute. The transition is amenable to probing through a direct laser excitation from the $^3P_0$ ground state. Because of a range of issues, this transition has not yet been comprehensively investigated in experiments. There is almost a gigahertz uncertainty in frequency determination [43] before some relative measurements performed by recent experiments.

Here we present the measurement results of the ultranarrow $6s6p^3P_0 - 4f^{13}5d6s^2$ $(J = 2)$ transition in ^{171}Yb atoms achieved through direct optical excitation. We conduct normalized spectroscopy on an ultracold ytterbium sample and determine the resonance frequency using an optical frequency comb referenced to an ultrastable optical cavity, and concurrently, the transition frequency is traced to the secondary representation of the SI second. A detailed calculation and measurement of the predominant systematic shifts, which include lattice light and the Zeeman effect, are performed, resulting in a total uncertainty of approximately 5 kHz. The accuracy of the measurement is constrained by the linewidth of transition spectra attributable to the Zeeman shift and optical lattice Stark shift. The determined magnetic sensitivities (Zeeman shifts) of the $4f^{13}5d6s^2$ $(J = 2)$ state are in good agreement with theoretical values. The electric-dipole ($E1$) magic wavelengths, hyperpolarizabilities, and tensor polarizabilities of the 1695-nm transitions are also roughly determined, displaying reasonable concordance with recent theoretical forecasts. The measured hyperfine splitting of the $4f^{13}5d6s^2$ $(J = 2)$ state exhibits an approximately sixfold enhancement in uncertainty reduction compared with the recent experimental findings. These measurements pave the way for future utilizations of the ^{171}Yb $6s6p^3P_0 - 4f^{13}5d6s^2$ $(J = 2)$ clock transition in significant applications such as searches for variation of α and violation of the Einstein equivalence principle, the examination of local Lorentz invariance, and the investigation of new light force carriers [38,39].

II. TRANSITION SPECTRUM DETECTION

The relevant energy levels of the ^{171}Yb atom are depicted in Fig. 1(a), and the measurement cycle, along with the detailed pulse sequence of the readout procedure, are shown in Appendix A. The experimental apparatus used in our experiment is essentially the same as that used previously [12,44], and a schematic drawing of that is depicted in Fig. 1(b). Full details concerning the cooling and trapping system employed in this work are discussed in previous publications [44,45].

After preparing atoms on the $6s6p^3P_0$ state using 578 nm laser in a one-dimensional (1D) lattice, we interrogate the $6s6p^3P_0 - 4f^{13}5d6s^2$ $(J = 2)$ transition with a specifically polarized 1695-nm laser pulse, the atoms at different Zeeman-sublevel state $^3P_0$, $m_F = \pm 1/2$ can be

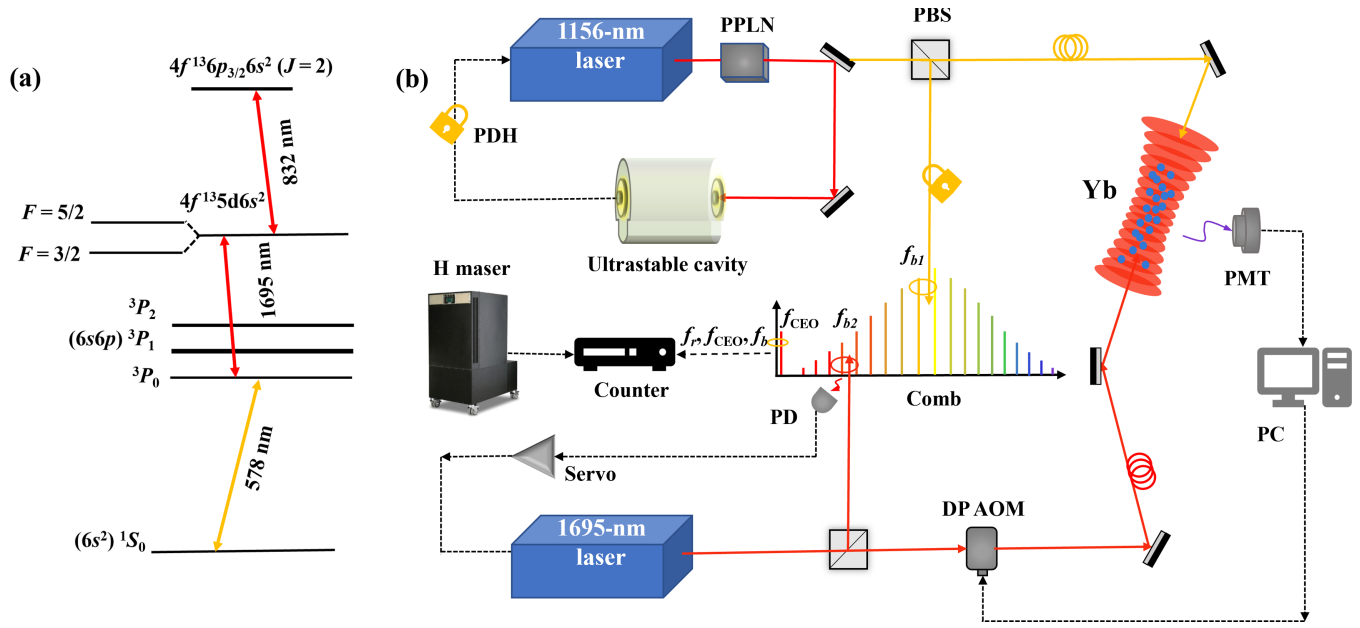

FIG. 1. (a) Partial energy-level diagram of a ^{171}Yb atom and the relevant transitions. (b) Schematic diagram of the experimental system. Double-passed acousto-optic modulator (DP AOM), polarization beam splitter (PBS), optical frequency comb (OFC), photodetector (PD), Pound-Drever-Hall method (PDH), photomultiplier tube (PMT), periodically poled lithium niobate (PPLN), carrier-envelope offset frequency of the comb (f_{CEO}), beat note between the comb and the laser (f_b), and repetition frequency (f_r). The frequency of the 1695-nm laser is locked and measured by an Er-doped femtosecond fiber frequency comb that is referenced to an ultrastable optical cavity.

excited, respectively. A bias magnetic field B is applied to define the quantization axis, parallel to both the lattice and the 1695-nm clock polarization vectors. Before starting the 1695-nm clock interrogations, a 20-ms delay is implemented to permit the decay of any transient magnetic fields to background levels. Rabi spectroscopy is performed on the π components of the transition using a 200-ms, 1695-nm laser pulse. The excitation fraction is determined from the laser-induced fluorescence, and a normalized scheme is employed with the 649-, 770-, and 592-nm lasers [44,46] (see Appendix A for details). The 1695-nm laser is locked to a commercial Er-doped femtosecond fiber frequency comb (Menlo Systems) with a repetition frequency of approximately 250 MHz, and the comb is referenced to an ultrastable optical cavity yielding an instability of less than 1×10^{-15} at 1-s averaging time [47]. Meanwhile, the recorded repetition rate and carrier offset frequencies are calibrated against the stabilized H maser featuring an instability (Allan deviation) of approximately 1×10^{-13} for integration times of 1 s, while the finally measured frequencies are calibrated utilizing the reference frequency of our ^{171}Yb $6s^2{}^1S_0 - 6s6p^3P_0$ clock transition. An acousto-optic modulator (AOM) is used to bridge the detuning between the 1695-nm laser and the atomic transition. By scanning the frequency of the AOM, the spectra of the $6s6p^3P_0 - 4f^{13}5d6s^2$ $(J=2)$ transition are obtained, as depicted in Fig. 2. The population of the atomic states is detected using a photomultiplier tube (PMT) with the application of an electron shelving technique for fluorescence detection.

This spectroscopy interrogation of the $^3P_0$-$J=2$ transition in ^{171}Yb is performed in a 1D optical lattice, effectively eliminating the predominant frequency shifts and line broadening due to the Doppler effect. The transition is electric quadrupole allowed and has typical natural linewidths of a few millihertz and saturation intensities of a few pW/cm^2. To obtain the best signal-to-noise ratio of the transition spectra, the 1695-nm probe pulse (traveling wave) is applied along the axial direction of the optical lattice with a power of about 0.5 mW, which is much larger than the saturation intensity. Based on theoretical prediction [38], a magic wavelength is anticipated to lie between 792 and 833 nm. Consequently, the lattice wavelength is finely adjusted within this interval to ascertain the magic wavelength. Figure 2(a) displays the Zeeman components of the hyperfine-structure transition at 1695 nm, specifically between the $F=1/2$ and $F=3/2$ levels. The obtained transition spectra presented in Figs. 2(b) and 2(c) reveal a noticeable energy differences among the $F=3/2$, $|m_F|=1/2$, and $|m_F|=3/2$ levels due to the optical lattice shift. Figure 2(d) shows the excitation profile of the $F=1/2$, $|m_F|=1/2$ to $F=3/2$, $|m_F|=1/2$ Zeeman components of the $6s6p^3P_0 - 4f^{13}5d6s^2$ $(J=2)$ hyperfine-structure transition under a

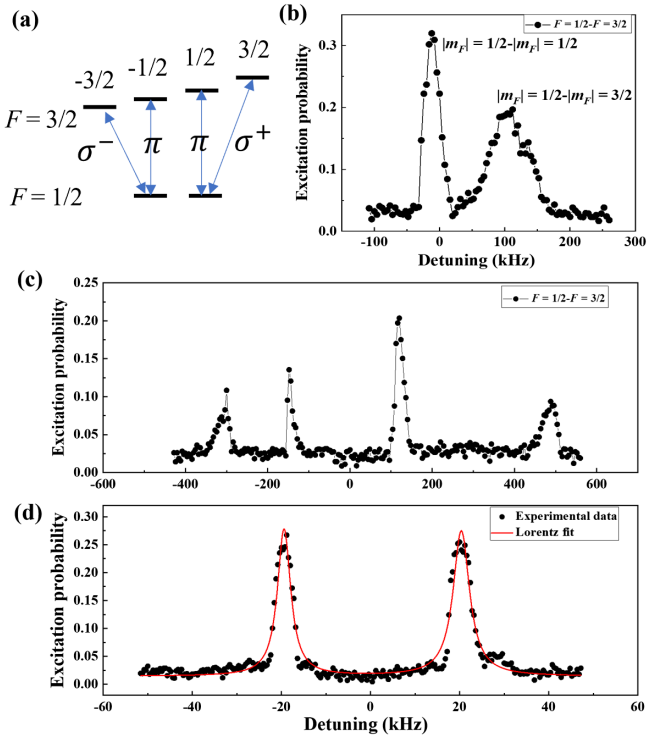

FIG. 2. High-resolution spectra of the ${}^3P_0(F = 1/2) - J = 2(F = 3/2)$ transition taken by scanning the frequency of the 1695-nm laser. (a) The $F = 1/2 - F = 3/2$ Zeeman component of the 1695-nm hyperfine-structure transition in the presence of a small-bias magnetic field. (b) The spectra are obtained under a quiet ambient magnetic field of less than 5 mG, a probe intensity of $I = 35\ \mathrm{mW/cm^2}$, and an interaction period of $\tau = 200$ ms. (c) Excitation probability as a function of the clock-laser detuning from the center of the $|\Delta m_F| = 0$ lines, showing the observed four individual Zeeman components with a static magnetic field $B_0 = 0.105$ G. The variations in excitation probabilities of the four components can be attributed to differences in state preparation and 592-nm pumping efficiencies. For all spectra in (b) and (c), the lattice wavelength is tuned to 831.6 nm. (d) The hyperfine-structure transition spectra of the $F = 1/2$, $|m_F| = 1/2$ to $F = 3/2$, $|m_F| = 1/2$ Zeeman components with a 0.016-G bias magnetic field. The observed linewidth of 4 kHz is constricted due to broadening effects caused by the optical lattice shift, which exhibits a lattice wavelength tuned to approximately 832.2 nm and a lattice power of 1 W. The solid curves represent Lorentzian line-shape fittings, which are employed to ascertain the center frequencies and the linewidths.

lattice wavelength of about 832.2 nm. The red curve shows a Lorentzian line-shape fitting, and the linewidth of the transition ($|\Delta m_F| = 0$) is nearly 4 kHz, which is much greater than its natural linewidth and is limited by the broadening from lattice light. Concurrently, the spectral line shape exhibits a degree of asymmetry and deviates slightly from the Lorentzian profile. This may originate from the motion of atoms along the lattice axis within the lattice potential, as well as from the higher-order contributions of polarizability [48,49]. To achieve further narrowing of the linewidth in the 1695-nm transition spectra, it is essential to prepare atoms in their longitudinal motional ground state, which is currently common practice in optical atomic clocks.

III. ZEEMAN SENSITIVITY DETERMINATION

The natural lifetime of the new clock state is significantly longer than the typical interrogation time, offering a potential for high stability and accuracy. However, the upper states considered in this work are associated with the $4f$-electron shell and possess a considerable total electronic angular momentum value, $J = 2$. This property suggests that they are more sensitive to external magnetic field and electric-field gradient than the other atomic species typically utilized in optical clocks. For bosonic isotopes, the impact of the Zeeman effect can be readily canceled out by employing the $m_F = 0 - m_F = 0$ transition. For the ^{171}Yb atom, the total atomic angular momentum F is a half-integer; hence, the state with zero m_F cannot exist. In standard optical clock operation, the first-order Zeeman shift is canceled by alternatingly probing two transitions with opposite values of m_F and averaging their transition frequencies. In the current transitions of ${}^3P_0$-$J = 2$, an electronic Zeeman shift occurs, characterized by an electronic Landé factor of 1.45 [43] and theoretical sensitivities to Zeeman splitting amounting to 2.45 and 1.63 $\mathrm{MHz/G}/m_F$ for the $F = 3/2$ and $F = 5/2$ hyperfine components, respectively. Such a high sensitivity results in the broadening of transition lines within a typical experimental environment where the background magnetic field fluctuates by approximately 1 mG in a short period. During the experiment, we apply an external magnetic bias field concomitant with the 1695-nm interrogation laser, and ascertain the field's magnitude through measurement of the 578-nm clock transition's Zeeman component spectra.

We assess the Zeeman sensitivity of the $J = 2$ state by changing the bias magnetic field, which allows us to calculate the linear Zeeman shift from the observed splitting between the Zeeman substates. We derive the linear Zeeman shift values of $2.44 \pm 0.05\ \mathrm{MHz/G}/m_F$ for the $F = 3/2$ state and $1.63 \pm 0.04\ \mathrm{MHz/G}/m_F$ for the $F = 5/2$ state, findings that correspond closely with theoretical predictions. The pertinent experimental results are displayed in Fig. 3 and Table I. Further details of the experimental setup and data processing are available in Appendix B.

IV. OPTICAL SHIFTS AND POLARIZABILITIES MEASUREMENT

The frequency shift of the clock transition due to the effect of the lattice laser field that traps the atoms is contingent upon the polarizabilities of the clock states. Optical lattice clocks have demonstrated that cancellation of trap perturbation leads to excellent clocks with

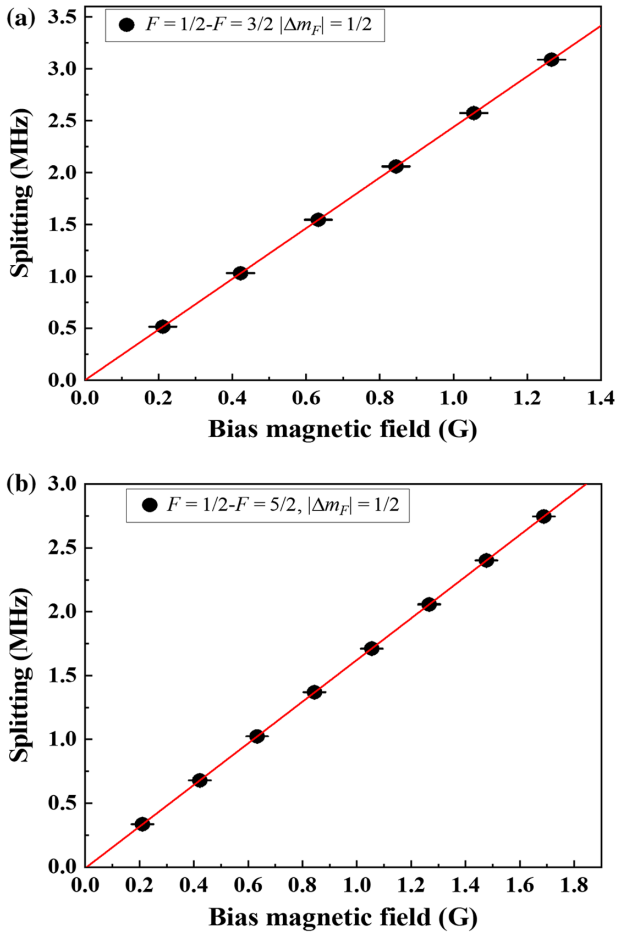

FIG. 3. The splitting of $m_F = \pm 1/2$ Zeeman substates versus external magnetic field for the (a) $F = 3/2$ and (b) $F = 5/2$ transitions. The obtained data (black points) are fitted by a linear function (red curves). The error bars are the standard error on the mean.

uncertainties less than the 10^{-18} level [50,51]. The concept of magic frequency trapping is proposed to equalize the polarizabilities of the clock states to realize the unperturbed atomic transition frequency while maintaining the experimental benefits of trapped systems [48]. Especially, the magic frequency concept becomes nontrivial for achieving high-accuracy clocks, when the contribution of the higher-order polarizabilities, including multipolarizabilities ($E2 - M1$) and hyperpolarizability [52,53], is nonnegligible compared to that of the $E1$ interaction. Taking into account the interrelation between the atomic temperature and trap depth, the lattice-light-induced shift around the magic wavelength can be written as

$$\delta v = -\Delta\alpha_{\xi F m_F}(v) I - \Delta\beta I^2, \tag{1}$$

where $\Delta_{\alpha\xi F m F v}(v) = \kappa^{E1}(v)\Delta v$, $\Delta\beta$ are the differences (denoted by Δ) of the $E1$ polarizability and hyperpolarizability on the clock-transition states, $\kappa^{E1}(v)$ is the linear coefficient of the $E1$ polarizability with respect to Δv, Δv is the detuning of lattice laser v from the $E1$ magic frequency v_m, and I is the intensity of the optical lattice.

In this experiment, we measure lattice light shifts of π transitions from the $^3P_0$ ($F = 1/2$) to $J = 2$ ($F = 3/2$ and $5/2$) states, respectively, and determine the $E1$ magic wavelengths and hyperpolarizabilities. Theoretical studies suggest that higher-order light shifts yield lattice-band-dependent effects that vary with atomic temperature [52,54], which is also the primary reason for the observed spectra broadening in current experimental conditions, as shown in Fig. 2. The total dipole polarizability of the state characterized by angular momentum $J = 2$ within a lattice laser field of frequency v that is linearly polarized and parallel to the quantization direction can be characterized as [55]

$$\Delta\alpha_{\xi F m_F}(\nu) = \Delta\alpha^S(\nu) + \frac{1}{2}\alpha^T_{J=2}(\nu)\frac{3{m_F}^2\text{-}F(F+1)}{F(2F-1)} \times (3\cos^2\theta\text{-}1), \tag{2}$$

where α^s and α^T are the dynamic scalar and tensor dipole polarizabilities, respectively, m_F is the projection of F, and θ is the angle between the bias magnetic field B and the lattice polarization vector $\in$. A large orbital momentum characterized by $J = 2$ leads to a considerably larger tensor Stark shift when compared with other species of the atomic optical clock. Consequently, during a typical measurement run, a bias magnetic field that is parallel to the lattice polarization vector is applied to ensure the stability of the tensor Stark value. Under these conditions, the light shifts are measured as a function of the lattice laser power across various lattice wavelengths, with subsequent quadratic extrapolation to the zero-intensity transition frequency being executed to delineate the ac Stark shifts attributed to the lattice light. The $E1$ polarizability induces a shift that exhibits a linear correlation with the trap depth, and the slope of the fitting lines when plotted as a function of the lattice frequency is illustrated in Figs. 4(b) and 4(e). From these data, the coefficients k_m^{E1} (the value of k^{E1} at the $E1$ magic wavelength) of $E1$ polarizabilities for the $F = 1/2 - F = 5/2$ and $F = 1/2 - F = 3/2$ transitions are ascertained to be 24.2 and 6.5 kHz/(THz W/cm^2), respectively, while the $E1$ magic wavelengths for these transitions are determined to be approximately 832.50 ± 0.04 and 832.24 ± 0.06 nm, respectively. The magic

TABLE I. The linear Zeeman shift slopes of different 1695-nm hyperfine transitions are obtained by theoretical calculation and experimental measurement, respectively.

States	This work	Theory
$F = 3/2$	2.44 ± 0.05 MHz/G/m_F	2.45 MHz/G/m_F
$F = 5/2$	1.63 ± 0.04 MHz/G/m_F	1.63 MHz/G/m_F

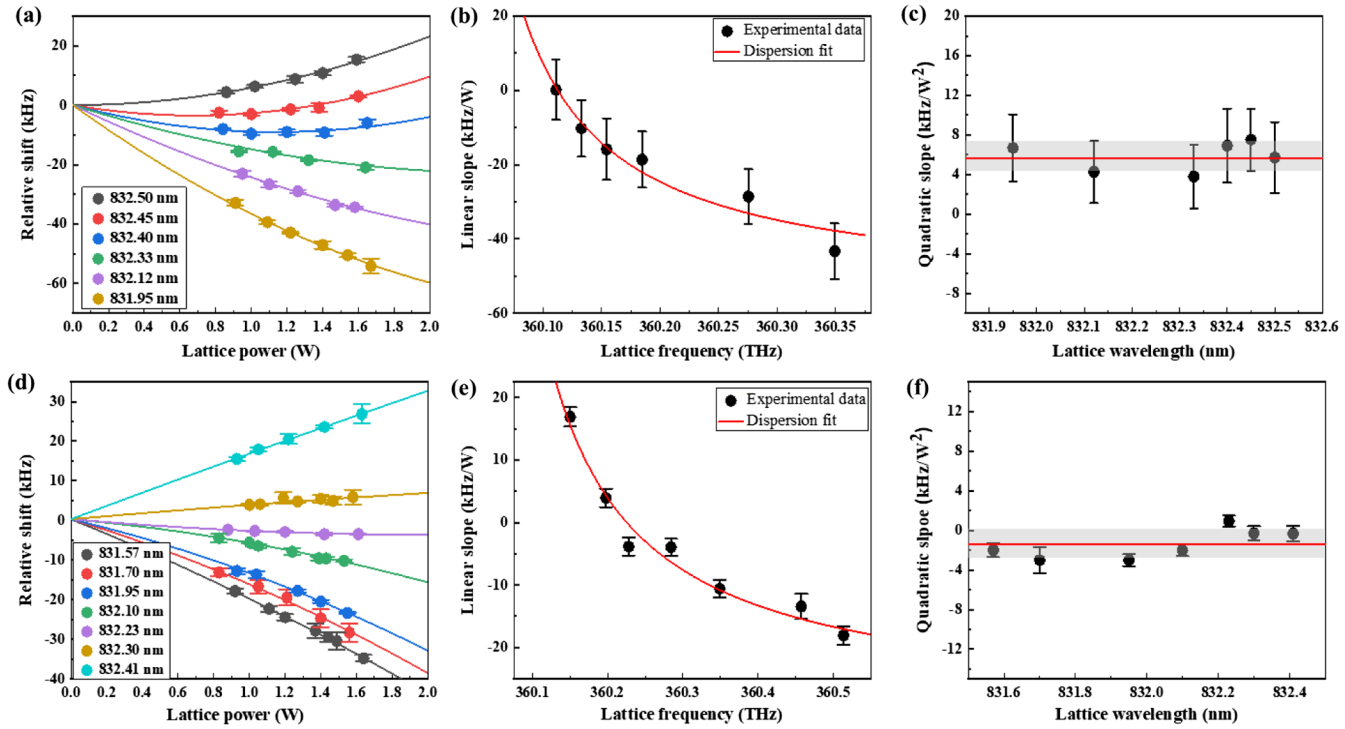

FIG. 4. Lattice light shifts and $E1$ magic frequency determination for the (a)–(c) $F = 1/2 - F = 5/2$ and (d)–(f) $F = 1/2 - F = 3/2$ transitions, respectively. All frequency data are offset by corresponding zero-intensity transition frequencies. The bias magnetic field parallels the lattice polarization vector during all measurements. The error bars in the graphs depict standard deviations. (a),(d) Relative clock shifts as a function of the lattice power at different lattice wavelengths. The solid lines are quadratic fits of the experimental data (colored points) using quadratic fitting. (b),(e) The dispersive slopes fitted from the optical shifts are plotted as a function of the lattice frequency. (c),(f) The quadratic slopes as a function of the lattice wavelengths.

wavelengths are very close to the $4f^{13}5d6s^2(J = 2) - 4f^{13}6p_{3/2}6s^2(J = 2)$ transition, accounting for this phenomenon of significant polarizabilities.

The hyperpolarizability induces a shift that exhibits a nonlinear scaling with trap depth. According to the fitting curves, the hyperpolarizabilities $\Delta\beta$ around the $E1$ magic wavelengths are quantified as approximately -13.1 ± 3.4 and 3.1 ± 3.4 Hz/(kW/cm^2)^2. These results exceed, by an order of magnitude greater than 5, the values reported for the ytterbium $^1S_0$-$^3P_0$ transition [56].

To evaluate the impact of the transition nearly resonant with the magic wavelength on the frequency of the 1695-nm transition, we tune the lattice frequency close to this resonance transition of $4f^{13}5d6s^2(J = 2) - 4f^{13}6p_{3/2}6s^2(J = 2)$ and measure the $6s6p^3P_0 - 4f^{13}5d6s^2(J = 2)$ optical shift [43]. As the lattice approaches the resonance, the spectral lines observed on the transition tend to become asymmetric and broadened. The light shifts associated with the transition under these conditions are illustrated in Fig. 5. Each point of lattice shift frequency is calculated from the average of six to eight measurements of the 1695-nm transition spectra centers, where the line shapes are fitted with a Lorentzian profile to determine the line center. The measured frequency shifts in relation to the lattice wavelengths are fitted with a dispersion line curve, from which the corresponding hyperpolarizabilities at the measured magic wavelengths are extrapolated to be -27 ± 27 and 2.5 ± 10 Hz/(kW/cm^2)^2, respectively. The results are consistent with the previous value at the 1σ level obtained by quadratic slopes.

The tensor polarizability of the $^3P_0$ state is nullified due to $J = 0$ and $m_F = 0$; thus, the tensor Stark shift of the 1695-nm transition is solely attributable to the $J = 2$ excited state. From Eq. (2), it is evident that the tensor polarizability of the $J = 2$ state is dependent on θ, and the rotation of the magnetic field results in distinct light shifts for every m_F state. Figure 6 illustrates the correlation between the tensor optical shift and θ. From this, the contribution due to the tensor Stark shift arising from the optical lattice can be assessed. The coefficients $\alpha^T_{j=2}$ of the tensor Stark shifts are determined to be -4.1 ± 0.3 and -2.2 ± 0.2 kHz/(kW/cm^2).

Based on the above measurements, it is apparent that the lattice light shift is a major contributor to the observed linewidth broadening due to the large dynamic polarizabilities. Therefore, measuring the transition in a shallow trap is an effective method to achieve a narrower transition spectrum. The fundamental reason for the broadening

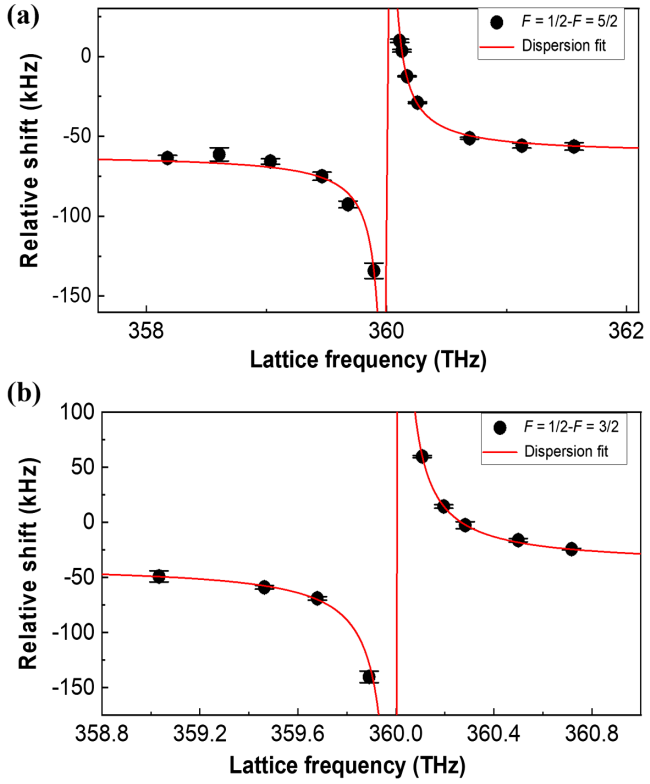

FIG. 5. ac Stark shifts on the 1695-nm transition with the lattice tuned near the $4f^{13}5d6s^2(J=2) - 4f^{13}6s^2 6p_{3/2}$ $(J=2)$ resonance transition with linear lattice polarization; all frequency data are offset by the zero-intensity transition frequencies from Figs. 4(a) and 4(d). Extrapolating the dispersion-shaped fit to the magic wavelength gives a shift of 11.7 and −1.3 kHz in 1- and 1.07-W lattice power for the (a) $F=1/2-F=5/2$ and (b) $F=1/2-F=3/2$ transitions, respectively. The error bars represent standard deviations.

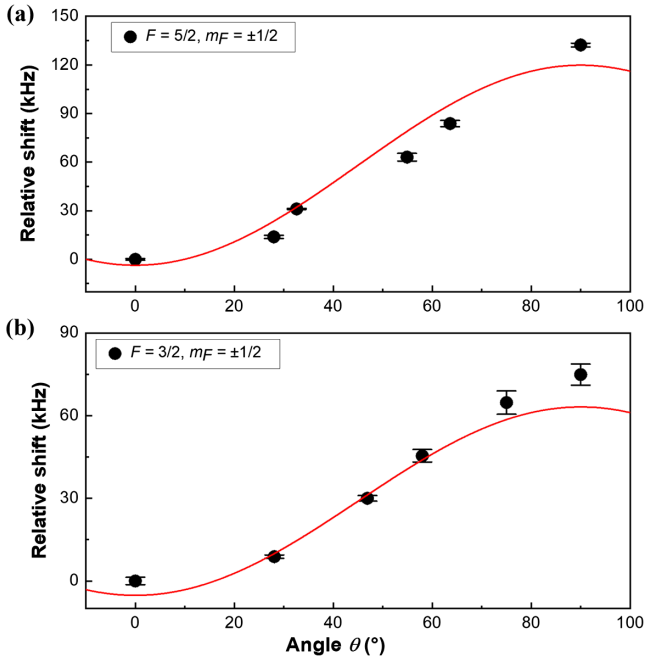

FIG. 6. The tensor Stark shifts on 1695-nm transitions under the condition that the quantization axis is parallel to the lattice polarization vector. The error bars are the standard error on the mean. (a) $^3P_0(F=1/2,m_F=\pm1/2)-J=2(F=5/2,m_F=\pm1/2)$ transition. (b) $^3P_0(F=1/2,m_F=\pm1/2)-J=2(F=3/2,m_F=\pm1/2)$ transition.

of the transition spectra by lattice light stems from the discrepancies in the optical shift among the different atoms in the lattice. We make a simple estimate of the optical lattice shift in a shallow lattice based on the parameters obtained. As the lattice shift correlates with both the lattice light frequency and intensity, it is feasible to find an appropriate lattice intensity that enables insensitivity of the lattice shift toward intensity fluctuations at a specific lattice frequency. When the lattice intensity is approximately at the 1-kW/cm^2 level and close to such a "magic intensity," the frequency shift fluctuation resulting from a typical optical lattice trap depth fluctuation is estimated to be less than 1 Hz. This indicates that the lattice light shift and the resulting linewidth broadening can be suppressed by the shallow lattice trap.

V. ABSOLUTE FREQUENCY AND HYPERFINE CONSTANTS

Our measured transition frequencies for all hyperfine components of $^3P_0$-$J=2$ are presented in Table II, in which the results are corrected for the dominant systematic frequency shifts, and the uncertainties consist of all major sources of errors. The accuracy attained in the measurements is on the order of 1 kHz, with the principal uncertainty arising from the lattice Stark shift (see Appendix D for more details).

The ^{171}Yb isotope, with a nuclear spin $I=1/2$, exhibits a distinct hyperfine structure, and the splitting interval of the $4f^{13}5d6s^2$ $(J=2)$ state is on the order of a few gigahertz. In a typical experiment, the 1695-nm probe laser incrementally scans the hyperfine transitions, and we subsequently derive the transition spectra and the absolute frequencies—a measurement of such precision that represents a first in experimental observations. The magnetic dipole constant A for the $4f^{13}5d6s^2$ $(J=2)$ state of ^{171}Yb has been determined as $A=112\,3252.3\pm 2.0$ kHz, with a further reduction in uncertainty compared to previous results in Table III. The measured ^{171}Yb $4f^{13}5d6s^2$ $(J=2)$ state hyperfine splitting is $280\,8130.8\pm4.9$ kHz, which is in good agreement with the recent experiment values [57,58], but improves the accuracy by 6 times more than the most accurate measurement result from Ref. [57]. The hyperfine shift is associated with the magnetic dipole and electric-quadrupole interactions, from which the hyperfine constant could be deduced.

TABLE II. Measured absolute frequencies of hyperfine components for the 1695-nm transition. The absolute frequencies of the two transitions in Ref. [57] are obtained by simply subtracting the known value for the frequency of the $4f^{14}6s^{2}{}^{1}S_0 - 4f^{14}6s6p^{3}P_0$ clock transition.

Transitions	$F = 1/2 - F = 5/2$	$F = 1/2 - F = 3/2$
This work	176 878 026 393.5 ± 4.7 kHz	176 875 218 262.7 ± 1.3 kHz
Ref. [57]	176 878 026 449 ± 31 kHz	176 875 218 266.2 ± 7.1 kHz

TABLE III. The comparison for $4f^{13}5d6s^2$ $(J = 2)$ hyperfine-structure constant of ^{171}Yb.

Interval	Magnetic dipole constant A	Reference
$4f^{13}5d6s^2$ $(J = 2)$	1 123 252.3 ± 2.0 kHz	This work
	1 124 640 ± 400 kHz	[46]
	1 123 300 ± 400 kHz	[58]
	1 123 273 ± 12 kHz	[57]

VI. CONCLUSION

In conclusion, we determine the frequencies of ^{171}Yb $6s6p^{3}P_0 - 4f^{13}5d6s^2$ $(J = 2)$ transitions with a standard uncertainty at the 1-kHz level using ultracold atoms and an optical frequency comb, which is the first time that the frequencies are directly measured in the experiment. According to the results, the hyperfine constant of ^{171}Yb for the $4f^{13}5d6s^2$ $(J = 2)$ state is obtained, and agrees well with other recent experimental results. In addition, the $E1$ magic wavelengths of the clock transitions are determined to be 832.50 ± 0.04 and 832.24 ± 0.06 nm for the $F = 1/2 - F = 5/2$ and $F = 1/2 - F = 3/2$ π transitions, respectively. The hyperpolarizabilities and tensor polarizabilities around the $E1$ magic wavelengths are also determined, which provides the data necessary for estimating the polarizabilities theoretically. The linear Zeeman shift slopes for the $F = 5/2$ and $F = 3/2$ transitions are also measured at 1.63 ± 0.04 and 2.44 ± 0.05 MHz/G/m_F and are consistent with the theoretical calculations. This work will prompt further investigation of the additional clock transition in ^{171}Yb and aligns with what has been achieved for the $^{1}S_0$-$^{3}P_0$ clock transition, and it also paves the way to high-precision measurements of relative frequency deviations between the two clock transitions. Together with the well-established $^{1}S_0$-$^{3}P_0$ transition, a suitable two-clock interrogation scheme may be implemented in the foreseeable future, which will help us further research the physics beyond the standard model, such as possible variations of the fine-structure constant and the effects arising from fundamental interactions.

ACKNOWLEDGMENTS

This work is supported by National Natural Science Foundation of China (Grants No. 62105102 and No. 11134003), National Key Research and Development Program of China (Grants No. 2016YFA0302103, No. 2017YFF0212003, and No. 2016YFB0501601), Shanghai Municipal Science and Technology Major Project (Grant No. 2019SHZDZX01), and Shanghai Excellent Academic Leaders Program (Grant No. 12XD1402400).

APPENDIX A: EXPERIMENTAL SETUP AND READOUT PROCEDURE

Loading, cooling, and imaging of ^{171}Yb atoms are described elsewhere. In brief, the frequency measurement cycle involves 400 ms of Doppler cooling, 200 ms of pumping at 578 nm, 200 ms of probing at 1695 nm, and 32 ms of readout pulses. The singlet transition of $^{1}S_0$-$^{1}P_1$ at 399 nm is used for 2D transverse cooling, Zeeman slowing, and blue magneto-optical-trap (MOT), cooling the atoms to an approximate temperature of 1 mK. Subsequently, the atoms are transferred to the narrow-linewidth ($\Gamma = 2\pi \times 182$ kHz) MOT that operates on the dipole-forbidden $^{1}S_0$-$^{3}P_1$ line at 556 nm, which cools the atoms to an estimated temperature of 10 μK. Following this, the sample is loaded to a 1D optical lattice with a waist radius of about 55 μm, generated by a continuous Ti: sapphire laser operating at approximately 830 nm. To probe transitions exciting from the $^{3}P_0$ state, a Rabi pulse from a high-frequency stabilized 578-nm laser, which coincides with the lattice laser, is utilized. The 578-nm laser of about 500 μW is sent to the atoms, yielding a transition spectrum with a typical linewidth (FWHM) of approximately 30 kHz. Subsequently, the frequency of the 578-nm laser is adjusted to match the point at which this transition exhibits the highest excitation fraction.

After excitation of the 1695-nm transition, we implement a dedicated readout procedure to realize the normalized detection. Each readout is destructive, and all observed atoms are removed from the lattice. The $^{1}S_0$-$^{1}P_1$ transition utilized for the first-stage laser cooling is employed to detect the fluorescence signal. The pump lasers are closely resonant with the corresponding transitions, the $F = 1/2 - F = 1/2$(649 nm), $F = 3/2 - F = 1/2$(770 nm), and $F = 3/2(5/2) - F = 3/2$(592 nm) hyperfine transitions are selected as the pumpers for "pumps 1, 2, 3," respectively. The relevant ytterbium levels are depicted in Fig. 7(a), and the sequence of readout pulses is illustrated in Fig. 7(b).

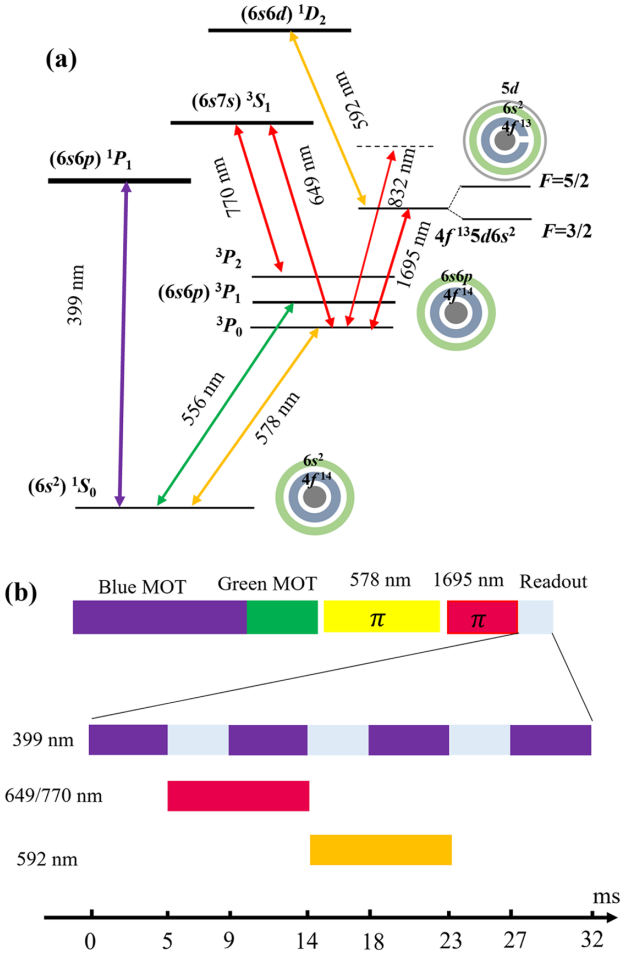

FIG. 7. (a) Energy levels and relevant transitions for ^{171}Yb. (b) Measurement cycle and detailed pulse sequence of the readout procedure. The PMT accumulates the fluorescence signal at 399 nm.

(a) First, a 5-ms, 399-nm resonant probe pulse is applied to measure the number of atoms remaining in the $^1S_0$ ground state after excitation by the 578-nm pulse, with the resulting signal designated as V_1.

(b) Second, employing two overlapping 9-ms, 649- or 770-nm pump pulses, the atoms remaining in the $^3P_0$ ground state after excitation by the 1695-nm pulse return to the ground state. Subsequently, a 5-ms, 399-nm pulse is employed to determine the number of atoms, with the signal being denoted by V_2.

(c) Third, a 5-ms, 592-nm resonant pulse is used to excite the atoms from the $4f^{13}5d6s^2$ $(J = 2)$ state to the $6s6d^1D_2$ state and subsequently decay in steps to the ground state. Concomitantly, with a 5-ms, 399-nm pulse, the number of atoms is ascertained, and this measurement is labeled V_3.

(d) Finally, a 5-ms, 399-nm pulse is applied, and the background signal V_4 is obtained.

From these measurements, the excitation probability P of the 1695-nm transition is calculated as

$$P = \frac{V_3 - V_4}{V_2 + V_3 - 2V_4}. \tag{A1}$$

APPENDIX B: BIAS MAGNETIC FIELD CALIBRATION AND ZEEMAN SHIFT

In the experiment, precise determination of the bias magnetic field is essential. The magnitude of the magnetic field is deduced from the measured frequencies of the two clock transitions of $|^1S_0, m_F = 1/2\rangle - |^3P_0,\ m_F = 1/2\rangle$, and $|^1S_0, m_F = -1/2\rangle - |^3P_0, m_F = -1/2\rangle$ in ^{171}Yb at different bias coil currents. Utilizing the intervals in the

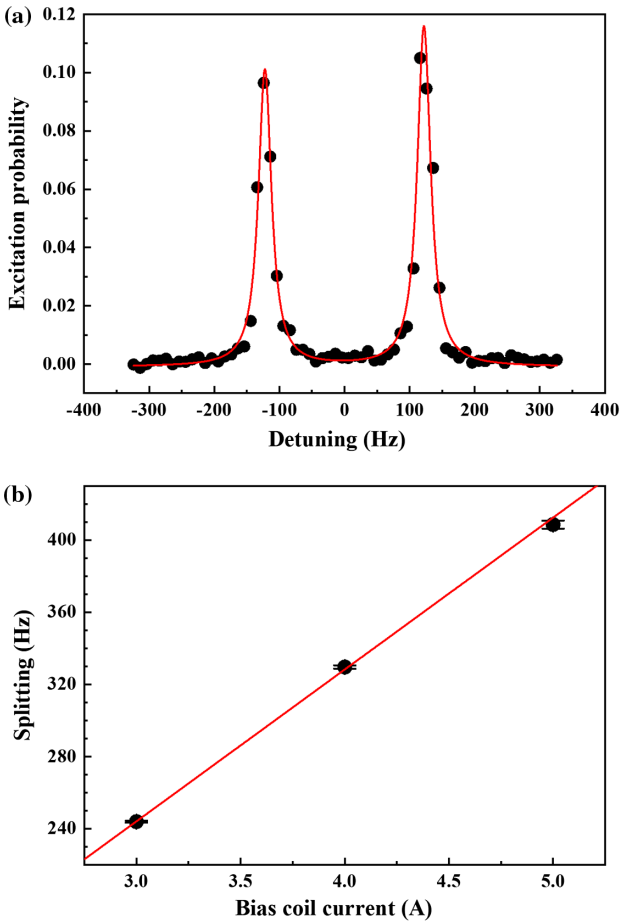

FIG. 8. Measurement of the bias magnetic field. (a) Normalized 578-nm clock-transition spectra of two π components under a bias coil current of 3 A. The red solid line indicates a Lorentzian double-peak fit utilized to ascertain the line center. (b) Relative intervals between the two π components correspond to the bias coil current. The red line is a linear fit of the experimental data. The error bars represent the standard deviations corresponding to the measured intervals.

578-nm transition spectrum and accounting for the established first-order Zeeman effect on the π transitions [6], we ascertain the correlation between the bias field magnitude and the coil current. As illustrated in Fig. 8(b), the linear Zeeman shift is 84.2 ± 1.9 Hz/A, which corresponds to 0.2110 ± 0.0046 G/A for the bias coil. Having determined the bias magnetic field's magnitude, the linear Zeeman sensitivities for the 1695-nm transitions are calculated: 2.44 ± 0.05 MHz/G/m_F for the $F = 3/2$ state and 1.63 ± 0.04 MHz/G/m_F for the $F = 5/2$ state, respectively. The calculation disregards the Zeeman shift of the $^3P_0$ state, as this shift, stemming from the nuclear Zeeman effect in the $^1S_0$-$^3P_0$ transition, is significantly smaller than the electronic Zeeman shift in the 1695-nm transition given our current measurement precision. The data agree well with the theoretical calculation, with the principal source of uncertainty arising from the determination of the bias magnetic field via the frequency measurements of the 578-nm clock transition.

In the 1695-nm transition, the magnitude of the second-order Zeeman effect surpasses that observed in other atomic optical clock species, rendering it non-negligible. According to Ref. [59], an atomic energy level characterized by electronic angular momentum J and nuclear spin $I = 1/2$, when subject to an external magnetic field B, is expressed as

$$E_{J,F=J\pm\frac{1}{2},m_F} = -\frac{1}{4}hA_J + g_J\mu_B B m_F \pm \frac{hA_J(2J+1)}{4}\sqrt{1 - \frac{8m_F(g_J\mu_B - g_I\mu_N)}{hA_J(2J+1)^2}B + \frac{4(g_J\mu_B - g_I\mu_N)^2}{[hA_J(2J+1)]^2}B^2}, \quad \text{(B1)}$$

where A_J is the hyperfine splitting constant, g_J and g_I are the electronic and nuclear Landé g factors, and μ_B and μ_N are the Bohr and nuclear magnetons, respectively.

The atomic energy-level shifts can be obtained from Eq. (B1),

$$E_{J,F=J\pm\frac{1}{2},m_F} = \frac{\pm(2J+1)-1}{4}hA_J + \left(1 \mp \frac{1}{2J+1}\right)g_J\mu_B m_F B \pm \left[\frac{1}{2} - \frac{1}{8}\left(\frac{4m_F}{2J+1}\right)^2\right]\frac{(g_J\mu_B - g_I\mu_N)^2}{hA_J(2J+1)}B^2, \quad \text{(B2)}$$

where the first term represents the hyperfine shift, whereas the subsequent terms correspond to the linear and quadratic Zeeman shifts, respectively.

For the $4f^{13}5d6s^2$ ($J = 2$), $m_F = \pm 1/2$ states, the level energy shifts can be expressed as

$$E_{F=\frac{3}{2},m_F} = -\frac{3}{2}hA_J + \frac{6}{5}g_J\mu_B m_F B - \left(\frac{1}{2} - \frac{2}{25}{m_F}^2\right)\frac{(g_J\mu_B - g_I\mu_N)^2}{5hA_J}B^2, \quad \text{(B3)}$$

$$E_{F=\frac{5}{2},m_F} = hA_J + \frac{4}{5}g_J\mu_B m_F B + \left(\frac{1}{2} - \frac{2}{25}{m_F}^2\right)\frac{(g_J\mu_B - g_I\mu_N)^2}{5hA_J}B^2. \quad \text{(B4)}$$

Consequently, the linear and quadratic Zeeman shift coefficients are calculable from Eqs. (B3) and (B4), as delineated in Table IV.

TABLE IV. The calculated linear and quadratic Zeeman shift coefficients.

States	Linear coefficients	Quadratic coefficients
$F = 3/2$	2.45 MHz/G/m_F	-142 Hz/G^2
$F = 5/2$	1.63 MHz/G/m_F	142 Hz/G^2

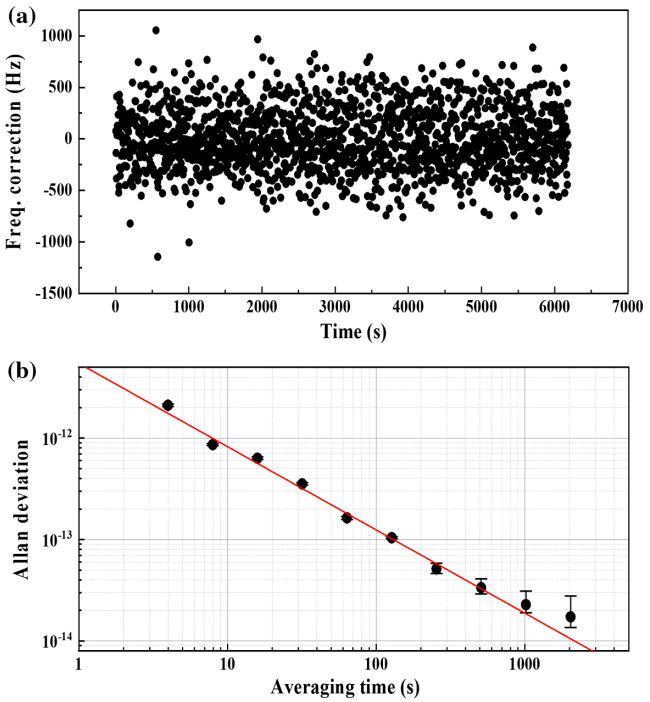

FIG. 9. A typical in-loop fractional frequency instability. (a) The frequency correction of 1695 nm during the closed-loop operation. (b) The stability of the atomic clock signal is quantified in terms of the Allan deviation of fractional frequency fluctuations. For Rabi interrogation, we fit a fractional instability of $5.5 \times 10^{-12}/\tau^{0.82}$.

APPENDIX C: CLOSED-LOOP OPERATION OF 1695-NM OPTICAL TRANSITION

Using single Rabi pulses from a 1695-nm laser, we probe the $^3P_0 - J = 2$ clock transition and acquire excitation spectra with an approximate 4-kHz linewidth, as illustrated in Fig. 2(d). Subsequently, we perform a closed-loop operation of the clock. The two π transitions ($F = 1/2$, $m_F = \pm 1/2 - F = 1/2$, $m_F = \pm 1/2$) are alternately interrogated to cancel the first-order Zeeman shift. The corresponding frequency correction signal is then sent to the double-passed acousto-optic modulator to lock the 1695-nm laser on the clock transition. The in-loop error signal stability of the clock is determined to be $5.5 \times 10^{-12}/\tau^{0.82}$, as depicted in Fig. 9, which is limited by the fluctuation of the background magnetic field. Additional narrowing of the 1695-nm transition spectra linewidth is anticipated to enhance the operational stability of the clock.

APPENDIX D: SYSTEMATIC SHIFTS AND ABSOLUTE FREQUENCY CALIBRATION

In our experiment, the predominant systematic shift and uncertainty originate from the optical lattice, which has a much larger effect than other systematic effects on the 1695-nm transition. Factors such as BBR, atomic collisions, and the ac Stark shift from the 1695-nm laser are estimated to exert negligible influence within the current frequency measurement accuracy [39]. Uncertainty arising from the Zeeman effect is also disregarded due to the interrogation of the two peaks. We investigate the influence of the 1695-nm probe power on the transition frequency in a similar scheme by varying the 1695-nm power. Statistical uncertainty is deduced from the standard deviation of the mean transition center obtained.

TABLE V. Uncertainty budget for the absolute frequency measurement of the 1695-nm clock transition.

	$F = 1/2 - F = 5/2$		$F = 1/2 - F = 3/2$	
Effects	Shifts (kHz)	Uncertainty (kHz)	Shifts (kHz)	Uncertainty (kHz)
Second-order Zeeman	<0.01	<0.01	<0.01	<0.01
Lattice light	6.3	4.5	4.1	0.8
Probe light	−1.6	0.6	0.9	0.2
Fiber transmission	0	1	0	1
H maser	0.51	0.16	0.51	0.16
Statistics	0	0.5	0	0.4
Total	5.2	4.7	5.5	1.4

A commercial Er-doped femtosecond fiber frequency comb referenced to a 1156-nm ultrastable optical cavity is employed for the stabilization of the 1695-nm laser. During the experiment, the repetition frequency, offset frequency, and beat note frequency from the comb and the 1695-nm laser are meticulously recorded using a K + K counter, which is calibrated against an H maser. The 578-nm optical clock frequency data obtained from the comb, in reference to the H maser, are calibrated against the absolute frequency of the $^1S_0$-$^3P_0$ transition [12]. For each measurement, 578-nm transition spectroscopy with Hz-level precision is deployed to ascertain the frequency difference between the observed 578-nm transition frequency via the comb and its absolute frequency.

Subsequent to the calculations, the disparity between the comb measurements and the absolute frequency of the 578-nm transition is approximately 1.5 kHz, necessitating a −0.5-kHz frequency correction for the 1695-nm transition frequencies. Moreover, the uncertainty engendered by the optical-fiber transmission within the optical chain is estimated to be less than 1 kHz. The total uncertainty budget for the measurement is presented in Table V. Consequently, the absolute frequencies of the $6s6p^3P_0 - 4f^{13}5d6s^2(J = 2)$ transition in ^{171}Yb are ascertained to be 176 878 026 393.5 ± 4.7 kHz and 176 875 218 262.7 ± 1.3 kHz corresponding to the $F = 1/2 - F = 5/2$ and $F = 1/2 - F = 3/2$ hyperfine transitions, respectively.

APPENDIX E: CHARACTERISTICS OF ^{171}Yb IN OPTICAL LATTICES OF MAGIC FREQUENCIES

From the experimentally determined data, such as the waist size of the optical lattice, the lattice power and the polarizabilities, the characteristics of ^{171}Yb in optical lattice of magic frequencies are calculated, as presented in Table VI.

TABLE VI. Characteristics of ^{171}Yb in optical lattices of magic frequencies.

λ_{clock} (nm)	1695	
Levels	$F = 5/2 m_F = \pm 1/2$	$F = 3/2 m_F = \pm 1/2$
λ_{m} (nm)	832.50	832.24
$k_m^{E1}\left(\frac{\text{kHz}}{(\text{kW/cm}^2)\cdot\text{THz}}\right)$	24.2	6.5
$\beta_m\left(\frac{\text{Hz}}{(\text{kW/cm}^2)^2}\right)$	−13.1	3.1
$\alpha_T\left(\frac{\text{kHz}}{\text{kW/cm}^2}\right)$	−4.1	−2.2

[1] J. Stenger, T. Binnewies, G. Wilpers, F. Riehle, H. R. Telle, J. K. Ranka, R. S. Windeler, and A. J. Stentz, *Phase-coherent frequency measurement of the* Ca *intercombination line at 657 nm with a Kerr-lens mode-locked femtosecond Laser*, Phys. Rev. A **63**, 021802 (2001).

[2] M. Takamoto, F. L. Hong, R. Higashi, and H. Katori, *An optical lattice clock*, Nature (London) **435**, 321 (2005).

[3] N. D. Lemke, A. D. Ludlow, Z. W. Barber, T. M. Fortier, S. A. Diddams, Y. Jiang, S. R. Jefferts, T. P. Heavner, T. E. Parker, and C. W. Oates, *Spin-1/2 optical lattice clock*, Phys. Rev. Lett. **103**, 063001 (2009).

[4] H. Hachisu, K. Miyagishi, S. G. Porsev, A. Derevianko, V. D. Ovsiannikov, V. G. Pal'chikov, M. Takamoto, and H. Katori, *Trapping of neutral mercury atoms and prospects for optical lattice clocks*, Phys. Rev. Lett. **100**, 053001 (2008).

[5] A. P. Kulosa, D. Fim, K. H. Zipfel, S. Ruhmann, S. Sauer *et al.*, *Towards a* Mg *lattice clock: Observation of the* $^1S_0 - {}^3P_0$ *transition and determination of the magic wavelength*, Phys. Rev. Lett. **115**, 240801 (2015).

[6] W. F. McGrew, X. Zhang, R. J. Fasano, S. A. Schäffer, K. Beloy *et al.*, *Atomic clock performance enabling geodesy below the centimetre level*, Nature (London) **564**, 87 (2018).

[7] T. Takano, M. Takamoto, I. Ushijima, N. Ohmae, T. Akatsuka *et al.*, *Geopotential measurements with synchronously linked optical lattice clocks*, Nat. Photonics **10**, 662 (2016).

[8] H. Kim, M. S. Heo, C. Y. Park, D. H. Yu, and W. K. Lee, *Absolute frequency measurement of the* ^{171}Yb *optical lattice clock at KRISS using TAI for over a year*, Metrologia **58**, 055007 (2021).

[9] M. Pizzocaro, F. Bregolin, P. Barbieri, B. Rauf, F. Levi, and D. Calonico, *Absolute frequency measurement of the* $^1S_0$-$^3P_0$ *transition of* ^{171}Yb *with a link to international atomic time*, Metrologia **57**, 035007 (2020).

[10] G. Mura, T. Franzen, C. A. Jaoudeh, A. Gorlitz, H. Luckmann *et al.*, *A transportable optical lattice clock using* ^{171}Yb, in *Proceedings of the Joint European Frequency and Time Forum & International Frequency Control Symposium (EFTF/IFC), Prague, Czech Republic* (2013), pp. 376–378, 10.1109/EFTF-IFC.2013.6702292.

[11] A. Zhang, Z. X. Xiong, X. T. Chen, Y. Y. Jiang, J. Q. Wang *et al.*, *Ytterbium optical lattice clock with instability of order* 10^{-18}, Metrologia **59**, 065009 (2022).

[12] L. M. Luo, H. Qiao, D. Ai, M. Zhou, S. Zhang *et al.*, *Absolute frequency measurement of an* Yb *optical clock at the* 10^{-16} *level using international atomic time*, Metrologia **57**, 065017 (2020).

[13] Y. Hisai, D. Akamatsu, T. Kobayashi, K. Hosaka, H. Inaba, F. L. Hong, and M. Yasuda, *Improved frequency ratio measurement with* ^{87}Sr *and* ^{171}Yb *optical lattice clocks at NMIJ*, Metrologia **58**, 015008 (2021).

[14] S. M. Brewer, J. S. Chen, A. M. Hankin, E. R. Clements, C. W. Chou, D. J. Wineland, D. B. Hume, and D. R. Leibrandt, $^{27}Al^+$ *quantum-logic clock with a systematic uncertainty below* 10^{-18}, Phys. Rev. Lett. **123**, 033201 (2019).

[15] T. Bothwell, D. Kedar, E. Oelker, J. M Robinson, S. L. Bromley, W. L. Tew, J. Ye, and C. J. Kennedy, *JILA SrI optical lattice clock with uncertainty of* 2.0×10^{-18}, Metrologia **56**, 065004 (2019).

[16] R. Lange, N. Huntemann, J. M. Rahm, C. Sanner, H. Shao, B. Lipphardt, Chr. Tamm, S. Weyers, and E. Peik, *Improved limits for violations of local position invariance from atomic clock comparisons*, Phys. Rev. Lett. **126**, 011102 (2021).

[17] Y. Huang, B. L. Zhang, M. Y. Zeng, Y. M. Hao, Z. X. Ma, H. Q. Zhang, H. Guan, Z. Chen, M. Wang, and K. L. Gao, *Liquid-nitrogen-cooled* Ca^+ *optical clock with systematic uncertainty of* 3×10^{-18}, Phys. Rev. Appl. **17**, 034041 (2022).

[18] M. Takamoto, I. Ushijima, N. Ohmae, T. Yahagi, K. Kokado, H. Shinkai, and H. Katori, *Test of general relativity by a pair of transportable optical lattice clocks*, Nat. Photonics **14**, 411 (2020).

[19] L. Sonderhouse, C. Sanner, R. B. Hutson, A. Goban, T. Bilitewski, L. F. Yan, W. R. Milner, A. M. Rey, and J. Ye, *Thermodynamics of a deeply degenerate* $SU(N)$*-symmetric Fermi gas*, Nat. Phys. **16**, 1216 (2020).

[20] H. Ozawa, S. Taie, Y. Takasu, and Y. Takahashi, *Antiferromagnetic spin correlation of* $SU(N)$ *Fermi gas in an optical superlattice*, Phys. Rev. Lett. **121**, 225303 (2018).

[21] F. Schäfer, T. Fukuhara, S. Sugawa, Y. Takasu, and Y. Takahashi, *Tools for quantum simulation with ultracold atoms in optical lattices*, Nat. Rev. Phys. **2**, 411 (2020).

[22] N. Schine, A. W. Young, W. J. Eckner, M. J. Martin, and A. M. Kaufman, *Long-lived Bell states in an array of optical clock qubits*, Nat. Phys. **18**, 1067 (2022).

[23] N. Yu and M. Tinto, *Gravitational wave detection with single-laser atom interferometers*, Gen. Relativ. Gravit. **43**, 1943 (2011).

[24] P. W. Graham, J. M. Hogan, M. A. Kasevich, and S. Rajendran, *New method for gravitational wave detection with atomic sensors*, Phys. Rev. Lett. **110**, 171102 (2013).

[25] S. Kolkowitz, I. Pikovski, N. Langellier, M. D. Lukin, R. L. Walsworth, and J. Ye, *Gravitational wave detection with optical lattice atomic clocks*, Phys. Rev. D **94**, 124043 (2016).

[26] T. E. Mehlstäubler, G. Grosche, Ch. Lisdat, P. O. Schmidt, and H. Denker, *Atomic clocks for geodesy*, Rep. Prog. Phys. **81**, 064401 (2018).

[27] J. Grotti *et al.*, *Geodesy and metrology with a transportable optical clock*, Nat. Phys. **14**, 437 (2018).

[28] T. Bothwell, C. J. Kennedy, A. Aeppli, D. Kedar, J. M. Robinson, E. Oelker, A. Staron, and J. Ye, *Resolving the gravitational redshift across a millimetre-scale atomic sample*, Nature (London) **602**, 420 (2022).

[29] S. Schiller, *Hydrogenlike highly charged ions for tests of the time independence of fundamental constants*, Phys. Rev. Lett. **98**, 180801 (2007).

[30] S. Blatt, A. D. Ludlow, G. K. Campbell, J. W. Thomsen, T. Zelevinsky *et al.*, *New limits on coupling of fundamental constants to gravity using* ^{87}Sr *optical lattice clocks*, Phys. Rev. Lett. **100**, 140801 (2008).

[31] R. M. Godun, P. B. R. Nisbet-Jones, J. M. Jones, S. A. King, L. A. M. Johnson, H. S. Margolis, K. Szymaniec, S. N. Lea, K. Bongs, and P. Gill, *Frequency ratio of two optical clock transitions in* $^{171}Yb^+$ *and constraints on the time variation of fundamental constants*, Phys. Rev. Lett. **113**, 210801 (2014).

[32] A. Derevianko and M. Pospelov, *Hunting for topological dark matter with atomic clocks*, Nat. Phys. **10**, 933 (2014).

[33] B. M. Roberts, G. Blewitt, C. Dailey, M. Murphy, M. Pospelov, A. Rollings, J. Sherman, W. Williams, and A. Derevianko, *Search for domain wall dark matter with atomic clocks on board global positioning system satellites*, Nat. Commun. **8**, 1195 (2017).

[34] H. Pihan-Le Bars, C. Guerlin, R.-D. Lasseri, J.-P. Ebran, Q. G. Bailey, S. Bize, E. Khan, and P. Wolf, *Lorentz-symmetry test at Planck-scale suppression with nucleons in a spin-polarized* ^{133}Cs *cold atom clock*, Phys. Rev. D **95**, 075026 (2017).

[35] C. Sanner, N. Huntemann, R. Lange, C. Tamm, E. Peik, M. S. Safronova, and S. G. Porsev, *Optical clock comparison for Lorentz symmetry testing*, Nature (London) **567**, 204 (2019).

[36] F. Riehle, P. Gill, F. Arias, and L. Robertsson, *The CIPM list of recommended frequency standard values: Guidelines and procedures*, Metrologia **55**, 188 (2018).

[37] J. Lodewyck, *On a definition of the SI second with a set of optical clock transitions*, Metrologia **56**, 055009 (2019).

[38] M. S. Safronova, S. G. Porsev, C. Sanner, and J. Ye, *Two clock transitions in neutral* Yb *for the highest sensitivity to variations of the fine-structure constant*, Phys. Rev. Lett. **120**, 173001 (2018).

[39] V. A. Dzuba, V. V. Flambaum, and S. Schiller, *Testing physics beyond the standard model through additional clock transitions in neutral ytterbium*, Phys. Rev. A **98**, 022501 (2018).

[40] J. J. Cheng, K. L. Jiang, and L. X. He, *Suppress blackbody radiation shift with two clock ytterbium clock transition*, Wuhan Univ. J. Nat. Sci. **24**, 427 (2019).

[41] V. I. Yudin, A. V. Taichenachev, M. Yu. Basalaev, O. N. Prudnikov, H. A. Fürst, T. E. Mehlstäubler, and S. N. Bagayev, *Combined atomic clock with blackbody-radiation-shift-induced instability below* 10^{-19} *under natural environment conditions*, New J. Phys. **23**, 023032 (2021).

[42] V. V. Flambaum and V. A. Dzuba, *Search for variation of the fundamental constants in atomic, molecular, and nuclear spectra*, Can. J. Phys. **87**, 25 (2009).

[43] Yu. Ralchenko, A. Kramida, J. Reader, and NIST ASD Team, *NIST Atomic Spectra Database* (version 4.1), National Institute of Standards and Technology, 2011, http://physics.nist.gov/asd.

[44] Q. Gao *et al.*, *Systematic evaluation of a* ^{171}Yb *optical clock by synchronous comparison between two lattice systems*, Sci. Rep. **8**, 8022 (2018).

[45] D. Ai *et al.*, *Study of optical clocks based on ultracold* ^{171}Yb *Atoms*, Chin. Phys. B **29**, 090601 (2020).

[46] W.-G. Jin, T. Horiguchi, M. Wakasugi, T. Hasegawa, and W. Yang, *Systematic study of isotope shifts and hyperfine structures in* YbI *by atomic-beam laser spectroscopy*, J. Phys. Soc. Jpn. **60**, 2896 (1991).

[47] S. Zhang, H. Qiao, D. Ai, M. Zhou, and X. Y. Xu, *Frequency stabilization of multiple wavelength lasers based on a broadband spectrum*, Laser Phys. Lett. **19**, 095701 (2022).

[48] H. Katori, M. Takamoto, V. G. Pal'chikov, and V. D. Ovsiannikov, *Ultrastable optical clock with neutral atoms in an engineered light shift trap*, Phys. Rev. Lett. **91**, 173005 (2003).

[49] A. V. Taichenachev, V. I. Yudin, V. D. Ovsiannikov, V. G. Pal'chikov, and C. W. Oates, *Frequency shifts in an optical lattice clock due to magnetic-dipole and electric-quadrupole transitions*, Phys. Rev. Lett. **101**, 193601 (2008).

[50] I. Ushijima, M. Takamoto, and H. Katori, *Operational magic intensity for* Sr *optical lattice clocks*, Phys. Rev. Lett. **121**, 263202 (2018).

[51] K. Kim, A. Aeppli, T. Bothwell, and J. Ye, *Evaluation of lattice light shift at low* 10^{-19} *uncertainty for a shallow lattice* Sr *optical clock*, Phys. Rev. Lett. **130**, 113203 (2023).

[52] V. D. Ovsiannikov, V. G. Pal'chikov, A. V. Taichenachev, V. I. Yudin, and H. Katori, *Multipole, nonlinear, and anharmonic uncertainties of clocks of* Sr *atoms in an optical lattice*, Phys. Rev. A **88**, 013405 (2013).

[53] H. Katori, K. Hashiguchi, E. Y. Il'inova, and V. D. Ovsiannikov, *Magic wavelength to make optical lattice clocks insensitive to atomic motion*, Phys. Rev. Lett. **103**, 153004 (2009).

[54] H. Katori, V. D. Ovsiannikov, S. I. Marmo, and V. G. Palchikov, *Strategies for reducing the light shift in atomic clocks*, Phys. Rev. A **91**, 052503 (2015).

[55] A. Derevianko and H. Katori, *Colloquium: Physics of optical lattice clocks*, Rev. Mod. Phys. **83**, 331 (2011).

[56] R. C. Brown, N. B. Phillips, K. Beloy, W. F. McGrew, M. Schioppo *et al.*, *Hyperpolarizability and operational magic wavelength in an optical lattice clock*, Phys. Rev. Lett. **119**, 253001 (2017).

[57] A. Kawasaki, T. Kobayashi, A. Nishiyama, T. Tanabe, and M. Yasuda, *Observation of the* $4f^{14}6s^2{}^1S_0 - 4f^{13}5d6s^2(J=2)$ *clock transition at 431 nm in* ^{171}Yb, Phys. Rev. A **107**, L060801 (2023).

[58] T. Ishiyama, K. Ono, T. Takano, A. Sunaga, and Y. Takahashi, *Observation of an inner-shell orbital clock transition in neutral ytterbium atoms*, Phys. Rev. Lett. **130**, 153402 (2023).

[59] A. A. Golovizin, D. O. Tregubov, E. S. Fedorova, D. A. Mishin, D. I. Provorchenko, K. Yu. Khabarova, V. N. Sorokin, and N. N. Kolachevsky, *Simultaneous bicolor interrogation in thulium optical clock providing very low systematic frequency shifts*, Nat. Commun. **12**, 5171 (2021).